# Oxidative Dehydrogenation of Hydrocarbons by $V_3O_7^+$ Compared to Other Vanadium Oxide Species†

**Xavier Rozanska‡ and Joachim Sauer***

*Institut für Chemie, Humboldt Universität zu Berlin, Unter den Linden 6, D-10099 Berlin, Germany*

*Received: January 18, 2009; Revised Manuscript Received: April 13, 2009*

The oxidative dehydrogenation of propane and but-1-ene by $V_3O_7^+$ is examined using density functional theory. The mechanisms presented share crucial elementary steps with selective oxidation of C−H bonds by different transition metal oxide systems ranging from gas phase species to active sites of enzymes. The more favorable interaction between the olefin and the positively charged vanadium oxide cluster has a significant impact on the reaction mechanisms. With but-1-ene a [2 + 2] addition of the C−H bond onto the V═O site is most favorable, whereas for propane the initial step is H abstraction by the V═O bond. Comparison is made with other gas phase species ($VO_2^+$ and $V_4O_{10}$) and with models for vanadium oxide supported on silica.

## Introduction

Mass spectrometry is successfully used to examine the reactivity of metal or metal oxide clusters in the gas phase with the aim of getting insight in catalytic reactions of such species on the surface of a support.[1] Among others, selective oxidation reactions are of interest.[2,3] Mass spectrometry experiments require that clusters consisting of atoms that are likely to belong to the active part of a catalyst are generated. Their charge and size can be controlled. The reactions of these active site models with different substrates can be monitored and possible products identified, but a detailed understanding of the mechanism is achieved only in combination with quantum mechanical studies of the relevant potential energy surfaces.

We consider vanadium oxide cluster cations as models for the active components of common oxidation catalysts[4] and examine mechanisms for the oxidative dehydrogenation (ODH) of hydrocarbons. The generation of size-selected vanadium oxide cluster cations has been reported before,[5−7] and their stabilities and structures were theoretically investigated.[7−9] Reactions of these cations with hydrocarbons have also been studied, see ref 10 and references therein. Among the different vanadium oxide cluster cations, species containing only formal $V^V$ are of interest[9a] because they are close to the active species found on solid powder catalyst, namely, $V_2O_5$ supported on oxides.[4] Whereas the radical cations among them such as $V_4O_{10}^+$ show unusually high reactivity and abstract hydrogen even from methane,[11] more representative of surface species are closed-shell vanadium oxide cluster cations, $(V_2O_5)_nVO_2^+$ ($n = 0, 1,...$) such as $VO_2^+$ and $V_3O_7^+$. The reactions of the mononuclear $VO_2^+$ species with alkanes and alkenes have been thoroughly studied experimentally and theoretically,[12,13] and we focus here on $V_3O_7^+$ being the smallest polynuclear closed-shell $V^V$ species. We consider propane as the smallest alkane with a secondary CH bond[10] and compare it with but-1-ene as a hydrocarbon that binds more strongly with the cation.[10,14] For the reaction with but-1-ene, formal hydride transfer has also been observed as an additional reaction channel yielding $V_3O_7H$ and the butenylium cation, $C_4H_7^+$.[10b]

We examine the mechanisms related to the oxidative dehydrogenation (ODH) of propane and but-1-ene by $V_3O_7^+$ using density functional theory (DFT) and find agreement with mass spectrometric investigations.[10] Comparison with previous computational studies[15] of the propane ODH on supported $VO_x/SiO_2$ catalysts will provide detailed understanding of the similarities and differences of surface species and their gas phase models.

## Methods

The calculations used the hybrid B3LYP functional[16] with triple-ζ plus polarization basis sets (TZVP) on all atoms[17] and employed Turbomole 5.7.[18] Frequency calculations were made to confirm that the optimized structures are minima or transition structures (TS). Energies including zero point vibrational contributions ($E_0$) are reported, unless otherwise stated.

Unrestricted Kohn−Sham (UB3LYP) was used for systems with triplet spin states, and open-shell singlet states were treated within the broken-symmetry approach. The spin-projected energy for the low spin (singlet) state ($E_{sp}$) is calculated from the broken-symmetry energy ($E_{bs}$) and the energy of the triplet state at the geometry of the broken-symmetry state ($E_{tr//bs}$) according to[19]

$$E_{sp} = (2E_{bs} - \langle S^2\rangle_{bs}E_{tr//bs})/(2 - \langle S^2\rangle_{bs}), \qquad (1)$$

where $\langle S^2\rangle_{bs}$ is the expectation value of the total-spin operator of the broken-symmetry solution. When $\langle S^2\rangle_{bs}$ differs significantly from 1 and when eq 1 is applied to transition structures that connect closed and open-shell singlet structures, spin-projection may be less reliable and $E_{sp}$ and $E_{bs}$ may be considered as lower and upper limits of the true low-spin energy.[20,21] In these cases we will report average energies as $(E_{sp} + E_{bs})/2 \pm (E_{sp} - E_{bs})$ in the text and the reaction energy diagrams show the range between $E_{sp}$ and $E_{bs}$ as shaded areas.

For the open shell triplet and broken symmetry states, natural orbitals have been determined which show the localization of unpaired electrons on individual V sites or on the propyl/butenyl radical.

† Part of the "Walter Thiel Festschrift".

* Corresponding author. Fax: (+49)3020937136. E-mail: js@chemie.hu-berlin.de.

‡ E-mail: tgakxr@chem.tue.nl.

10.1021/jp9005235 CCC: $40.75 
Published on Web 05/13/2009

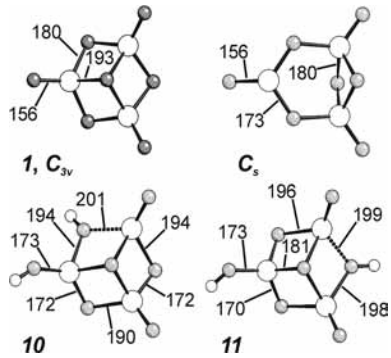


**Figure 1.** $V_3O_7^+$ (top) and $V_3O_7H_2^+$ (bottom) isomers with selected bond distances in pm.

The use of B3LYP (in connection with the broken symmetry approach) is supported by several previous studies.[9,15c,22−24] B3LYP reproduced experimental and CCSD(T) results for the dissociation of $VO_2^+$ into $VO^+$ and 1/2 $O_2$.[9] Good agreement between multireference calculations and B3LYP (broken-symmetry) results has also been found for the molecular structures of $V_2O_4$ and the relative energies of its open shell singlet and triplet states due to the coupling of the spins of two electrons in d states at the two V sites.[22a] Moreover, in contrast to both BLYP and BHLYP, B3LYP describes the size dependent localization of the extra electron in $(V_2O_5)_n^-$ anions properly.[22b] This emerged from comparison with both experimental vibrational spectra and CCSD(T) calculations.[22b] CCSD(T) single point calculations showed that, in contrast to GGA functionals, the B3LYP potential energy surfaces for the reactions of the smaller O═V(OH)$_3$ model with $C_3H_8$ is qualitatively correct.[15c] The B3LYP energy profile was found less pronounced with too unstable intermediates and too low barriers. Pykavy and van Wüllen have made a similar observation for the $CH_4$ + VO reaction.[23]

Classical transition state theory is used to calculate rate constants for elementary steps from free energy barriers. The partition functions are calculated within the rigid-rotor−harmonic oscillator−ideal gas model. In the present study this simple model is used only to get qualitative estimates of the relative importance of different steps.

## Results

The B3LYP structures of $V_3O_7^+$ have been reported before.[9,13b] Of the two isomers (Figure 1) the ring type $C_s$ structure is +24 kJ·mol$^{-1}$ less stable than the cagelike $C_{3v}$ structure with the 3-fold coordinated oxygen. The $C_{3v} \rightarrow C_s$ barrier is +32 kJ·mol$^{-1}$.

In the considered reaction, $[V^{(V)}{}_3O_7]^+$ undergoes reduction to $[V^{(V)}V^{(IV)}{}_2O_7H_2]^+$. Whereas $V_3O_7^+$ has a closed-shell singlet ground state, $V_3O_7H_2^+$ has two electrons in vanadium d states. When these electrons are on different vanadium sites, they form a diradical with high (triplet) or low spin (singlet) configuration. A triplet state with the two electrons on the same vanadium site, namely, $[V_2^{(V)}V^{(III)}O_7H_2]^+$, also exists but has a 52 kJ·mol$^{-1}$ higher energy. Therefore and because of the possibility of spin-crossing, we examine both the singlet and triplet potential energy surfaces of the ODH reaction, first for propane and then for but-1-ene. We do not present all reaction steps that have been investigated: transition structures with significantly higher free energies than others will result in negligible rate constants and are not shown. Considering the experimental reaction temperature of about $T$ = 298 K, a 20 kJ·mol$^{-1}$ higher Gibbs free energy of activation leads to a 3200 times smaller rate constant which is assumed to be sufficient to neglect the corresponding pathway compared to others from the same intermediate.

**Reactions with Propane.** Figure 2 shows the reaction pathways for propane (top) and the Gibbs free reaction energy profile (bottom). Figure 3 shows geometry details of selected structures, and the energies are reported in Table 1. Formation of the $V_3O_7^+ \cdot C_3H_8$ complex (**2**) is exothermic with $\Delta G_{298}$ = −63 kJ·mol$^{-1}$. The interaction with propane is so strong that the V-site of $V_3O_7^+$ to which propane binds gives up its coordination to the central O atom. The corresponding V−O distance changes from 193 to 340 pm and the structure of $V_3O_7^+$ from cage-type ($C_{3v}$) type to ring-type ($C_s$). A similar structure change is predicted for the formation of the $V_3O_7^+ \cdot$Ar complex.[9b] For the ring-type structure of the latter, evidence comes from infrared photodissociation spectra which show agreement with the B3LYP spectra for the $V_3O_7^+ \cdot$Ar (ring) complex, but not for the $V_3O_7^+ \cdot$Ar (cage) complex.[9b]

In the first step (TS **2/3**) hydrogen abstraction by the O═V$^+$(O−)$_2$ group from $C_3H_8$ yields the $C_3H_7^{\bullet} \cdot V_3O_7H^{+\bullet}$ diradical **3** which recombines to **4** through a rebound mechanism (TS **3/4**). Although the Gibbs free energy of **3** is higher than that of TS **3/4**, **3** corresponds to a minimum on the broken-symmetry potential energy surface. The electronic energy of TS **3/4** is 2 kJ·mol$^{-1}$ higher than that of **3** before spin projection (Table 1). The diradicaloid nature of **3** is confirmed when this structure is optimized imposing a triplet spin configuration: It gives the complex **12**. The electronic energy of **12** (−87 kJ·mol$^{-1}$) is indeed close to that of **3** (−71 kJ·mol$^{-1}$) before spin projection.

Figure 3 shows that structure **3** is similar to **4**, with the exception of an elongated C−V bond (249 instead of 200 pm). Due to the weaker C···V interaction in **3**, the $V_3O_7H$ part assumes a cage type structure with an additional V−O bond to the 3-fold coordinated O, whereas in **4** formation of the C−V bond has led to rupture of this V−O bond and the $V_3O_7H$ part assumes a ring-type structure. The existence of two minima along the V−C bond coordinate can be attributed to an avoided crossing of the potential energy surface for the dissociation of the C−V $\sigma$ bond into two $\sigma$ radicals, C−V → C$^{\bullet}$ + $^{\bullet}$V, and that for formation of the $[V_3O_7H^{+\bullet} \cdot C_3H_7^{\bullet}]$ pair from the separated radicals with the single electron on $[V_3O_7H]^{+\bullet}$ occupying a stable d orbital instead of a $\sigma$ hybrid orbital, thus creating a $V^{IV}(d^1)$ site.

A transition structure that connects directly **2** to **4** exists (TS **2/4**), but has a 20 ± 5 kJ·mol$^{-1}$ higher Gibbs free energy than TS **2/3**. The $E_0$ difference is 7 kJ·mol$^{-1}$, whereas the $E_{el}$ barriers are virtually the same (Table 1). This shows that the less constrained nature of the biradicaloid structure **2/3** compared to the structure **2/4** (Figure 3) favors the H abstraction/rebound path via **2/3** and **3/4** over the direct path through TS **2/4**, which corresponds to a [2 + 2] addition of the C−H on the V═O bond.

From the rather stable adduct **4** ($\Delta G_{298}$ = −199 kJ·mol$^{-1}$), in which the propyl group has attached to the vanadium atom, two pathways can be followed that involve direct abstraction of the second H atom from one of the methyl groups by a bridging oxygen atom accompanied by rupture of the C−V bond (TS **4/8**, see Figure 3, and TS **4/9**). This leads to formation of the C═C bond and completes the dehydrogenation of propane. The two transition structures differ only in the oxygen atom to which the H atom is transferred. The $E_0$ difference between them is only 7 kJ·mol$^{-1}$. The product complexes **8** and **9** dissociate into propene and species **10** and **11**, respectively (see Figure 1). The latter have both two weakly interacting electrons in d-shells

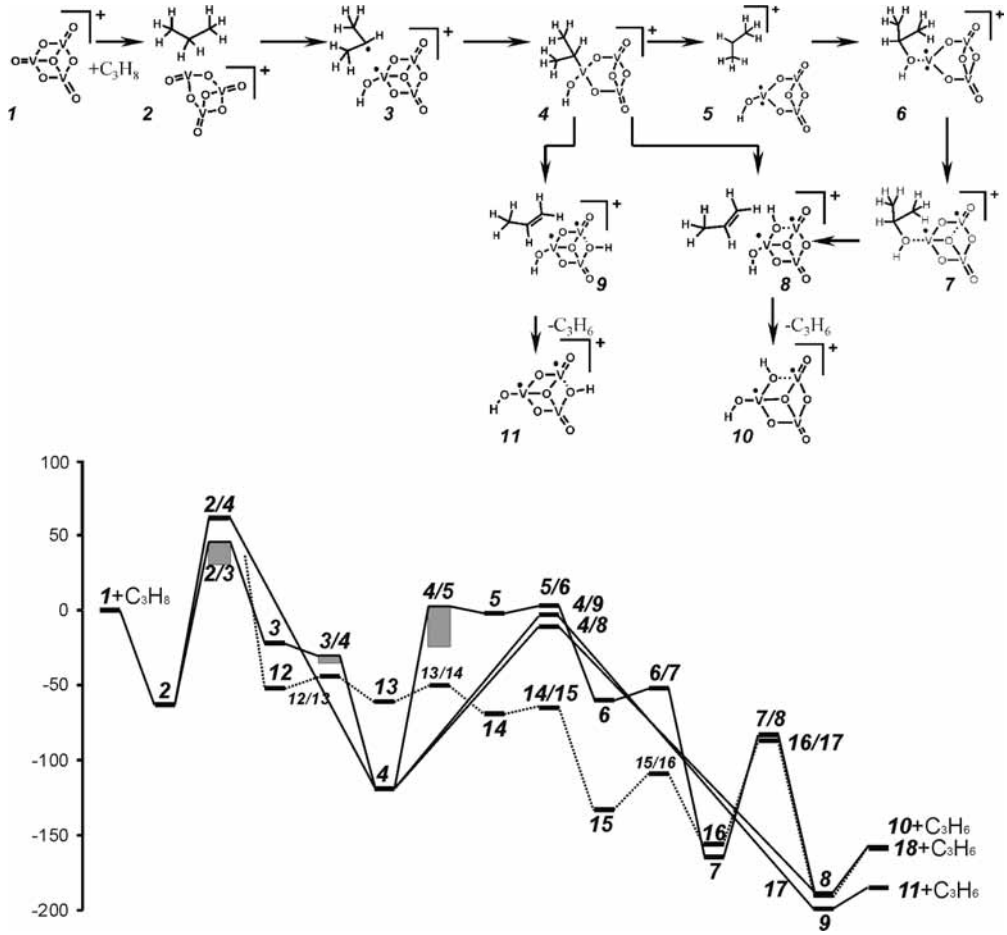


**Figure 2.** Reaction of propane with $V_3O_7^+$. Top: Singlet pathways. Bottom: Gibbs free energy (298 K) reaction diagrams. The full and broken lines connect the singlet and triplet structures, respectively. The values (axis in kJ·mol$^{-1}$) are also reported in Table 1. The shaded areas indicate uncertainty intervals between broken-symmetry (bs) and spin-projected energies (s) when $\langle S^2\rangle_{bs}$ differs significantly from 1.

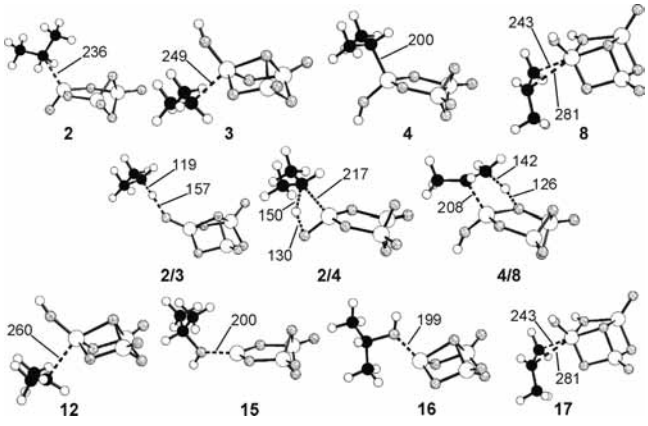


**Figure 3.** Geometry details of selected structures with distances in pm.

on two different vanadium atoms, but the two H atoms are at different oxygen positions.

There is a third pathway from **4** which is only found with the broken-symmetry approach. It involves dissociation of $[C_3H_7-V_3O_7H]^+$ into a complex between the propyl cation and the neutral $V_3O_7H^{\bullet\bullet}$ species with a $HO-V^{III}(O-)_2$ site that has two electrons in the vanadium d states, $C_3H_7^+ \cdot V_3O_7H^{\bullet\bullet}$ (**5**). Considering the Gibbs free energies in Table 1, the rate constant for the **4/5** path differs by factors of $8 \times 10^{-3}$ and $4 \times 10^{-2}$ from the rate constants for the **4/8** and **4/9** paths, which shows that the **4/5** path may play some role. Formally, **5** is the hydride transfer product of the reaction of propane with $V_3O_7^+$. It can dissociate into $V_3O_7H + C_3H_7^+$ with a Gibbs free energy change of $-78$ kJ·mol$^{-1}$ ($\Delta E_0 = -32$ kJ·mol$^{-1}$). The most stable singlet $V_3O_7H$ species has its two open shell electrons distributed over two vanadium sites: This is different from the $V_3O_7H$ unit

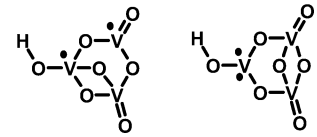

in **5** and also from the most stable triplet $V_3O_7H$ species which both have the two unpaired electrons on the same vanadium site (see the above formula on the right).

As alternative to dissociation, the much more stable ODH products **10** + $C_3H_6$ can be reached from **5** if the propyl cation rebinds to the HO−V group[25] (TS **5/6**) and forms *i*-propanol as part of an $[i\text{-}C_3H_7OH \cdot V_3O_6^{\bullet\bullet}]^+$ complex (**6**). Intermediate **5** represents a very shallow minimum on the singlet potential energy surface and can convert into **4** or **6** with free energy barriers of only 3 (TS **4/5**) or 5 kJ·mol$^{-1}$ (TS **5/6**), respectively. After reaching **6**, isomerization of $V_3O_6^{\bullet\bullet+}$ leads to structure **7**, in which the two electrons in vanadium d states are at different V sites. The Gibbs free energy barrier (TS **6/7**) is only 8 kJ·mol$^{-1}$, but complex **7** is significantly more stable than **6** and suitable for propene elimination from isopropanol in step **7/8**. This yields the same complex of propene with $V_3O_7H_2^{\bullet\bullet+}$ (**8**) that is also directly reached from **4** via TS **4/8**.

**TABLE 1: Energies and Total Spin for the Reaction of Propane with $V_3O_7^+$ [a]**

| label | $E_{el}$ | $E_0$ | $G_{298}$ | $\langle S^2\rangle$ | $E_{spe}^{tr}$ |
|---|---|---|---|---|---|
| **1** + $C_3H_8$ | 0 | 0 | 0 | −/− | −/− |
| **2** | −109 | −107 | −63 | − | − |
| TS **2/3** | $24^{bs}$, $13^{s}$ | $6^{bs}$, $-5^{s}$ | $44^{bs}$, $33^{s}$ | 0.59 | 50 |
| TS **2/4** | 23 | 13 | 59 | − | − |
| **3** | $-71^{bs}$, $-58^{s}$ | $-80^{bs}$, $-67^{s}$ | $-35^{bs}$, $-22^{s}$ | 1.00 | −84 |
| $V_3O_7H^{+\bullet}$ + $C_3H_7^{\bullet}$ | 48 | 33 | 28 | 0.76/0.75 | −/− |
| TS **3/4** | $-69^{bs}$, $-70^{s}$ | $-79^{bs}$, $-80^{s}$ | $-32^{bs}$, $-33^{s}$ | 0.76 | −68 |
| **4** | −161 | −165 | −119 | − | − |
| TS **4/5** | $-45^{bs}$, $-22^{s}$ | $-60^{bs}$, $-37^{s}$ | $-22^{bs}$, $1^{s}$ | 0.94 | −72 |
| TS **4/8** | −47 | −62 | −11 | − | − |
| TS **4/9** | −37 | −55 | −3 | − | − |
| **5** | $-58^{bs}$, $-24^{s}$ | $-71^{bs}$, $-37^{s}$ | $-36^{bs}$, $-2^{s}$ | 1.00 | −92 |
| $V_3O_7H^{\bullet\bullet}$ + $C_3H_7^+$ | $-57^{bs}$, $-56^{s}$ | $-74^{bs}$, $-73^{s}$ | $-81^{bs}$, $-80^{s}$ | 1.02/− | −57 |
| TS **5/6** | $-58^{bs}$, $-24^{s}$ | $-70^{bs}$, $-36^{s}$ | $-31^{bs}$, $3^{s}$ | 1.00 | −92 |
| **6** | $-139^{bs}$, $-104^{s}$ | $-134^{bs}$, $-99^{s}$ | $-96^{bs}$, $-60^{s}$ | 1.00 | −175 |
| TS **6/7** | $-120^{bs}$, $-100^{s}$ | $-115^{bs}$, $-95^{s}$ | $-72^{bs}$, $-52^{s}$ | 1.00 | −141 |
| **7** | $-217^{bs}$, $-217^{s}$ | $-211^{bs}$, $-211^{s}$ | $-165^{bs}$, $-165^{s}$ | 1.02 | −218 |
| TS **7/8** | $-122^{bs}$, $-119^{s}$ | $-131^{bs}$, $-128^{s}$ | $-85^{bs}$, $-83^{s}$ | 1.02 | −124 |
| **8** | $-232^{bs}$, $-231^{s}$ | $-236^{bs}$, $-235^{s}$ | $-190^{bs}$, $-189^{s}$ | 1.02 | −233 |
| **9** | $-239^{bs}$, $-238^{s}$ | $-244^{bs}$, $-243^{s}$ | $-200^{bs}$, $-199^{s}$ | 1.02 | −240 |
| **10** + $C_3H_6$ | $-149^{bs}$, $-148^{s}$ | $-157^{bs}$, $-156^{s}$ | $-159^{bs}$, $-158^{s}$ | 1.02/− | −149/ − |
| **11** + $C_3H_6$ | $-175^{bs}$, $-175^{s}$ | $-184^{bs}$, $-184^{s}$ | $-185^{bs}$, $-185^{s}$ | 1.03/− | −175/− |
| $V_3O_7^{+\bullet\bullet}$ + $C_3H_8$ | 173 | 169 | 233 | 2.01/− | −/− |
| **12** | −87 | −97 | −52 | 2.02 | − |
| TS **12/13** | −80 | −90 | −44 | 2.02 | − |
| **13** | −94 | −104 | −61 | 2.02 | − |
| TS **13/14** | −75 | −89 | −50 | 2.02 | − |
| **14** | −92 | −105 | −69 | 2.02 | − |
| $V_3O_7H^{\bullet\bullet}$ + $C_3H_7^+$ | −65 | −81 | −83 | 2.02/− | −/− |
| TS **14/15** | −92 | −104 | −64 | 2.02 | − |
| **15** | −176 | −171 | −133 | 2.01 | − |
| TS **15/16** | −158 | −153 | −109 | 2.02 | − |
| **16** | −209 | −202 | −156 | 2.01 | − |
| TS **16/17** | −124 | −133 | −87 | 2.02 | − |
| **17** | −233 | −237 | −190 | 2.02 | − |
| **18** + $C_3H_6$ | −150 | −158 | −159 | 2.02/− | − |

[a] $E_{el}$, $E_0$, $G_{298}$, and $E_{spe}^{tr}$ are the electronic energies, energies at 0 K, Gibbs free energies, and single point energy in the triplet state respectively. The energies are in kJ·mol$^{-1}$. For open-shell singlet systems, broken-symmetry (bs) and spin-projected (s) values are given (see eq 1). $\langle S^2\rangle$ is the expectation value of the total spin operator and is close to 1 and 2 for broken-symmetry and triplet states, respectively.

To discuss the *triplet potential energy surface*, we go back to the diradical intermediate **3** which consists of two weakly interacting subsystems with unpaired electrons, namely, $C_3H_7^{\bullet}$ and $V_3O_7H^{\bullet+}$. In **3** the two spins are coupled into an open-shell singlet, but they can also form a triplet, **12** (Figure 3), that has almost the same structure but a lower energy. The bottom part of Figure 3 and Figure 4 show the intermediates on the triplet path to propene. In intermediate **13** (Figure 4), the triplet equivalent of **4**, the electron pair of the C−V bond is decoupled and forms another $C_3H_7^{\bullet}\cdot V_3O_7H^{\bullet+}$ diradical which differs from **12** (Figure 3) by a shorter C···V bond distance, 238 vs 260 pm, and in the structure type of the $V_3O_7H$ part, ring (**13**) vs cage with 3-fold coordinated O (**12**).

Subsequently, electron transfer from the propyl species (TS **13/14**) leads to a propyl cation in the $C_3H_7^{+}\cdot{}^{t}V_3O_7H^{\bullet\bullet}$ complex (**14**) that is the triplet counterpart of the singlet intermediate **5**. Figure 4 shows substantial structural rearrangements from **13** via TS **13/14** to **14** that accompany the electron transfer. Unlike the propyl radical, the propyl cation is coordinated via two terminal C−H bonds to two O sites of the $V_3O_7H$ species. Figure 4 also shows the singly occupied natural orbitals. While one of the unpaired electrons occupies a vanadium d state in all three structures, **13**, **13/14** and **14**, the other is localized on the propyl radical in **13**, but occupies a second vanadium d orbital in **14**. Hence, the vanadium(IV) site in **13** is transformed into a vanadium(III) site in **14.**

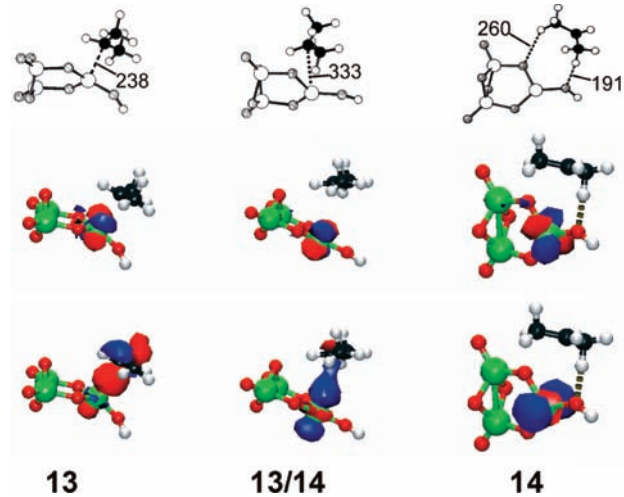


**Figure 4.** Geometric details (distances in pm) and the two singly occupied natural orbitals for structures connected by electron transfer from the propyl radical to $V_3O_7H^{+\bullet}$.

Intermediate **14** can either dissociate into the hydrid transfer products $C_3H_7^+$ and triplet $V_3O_7H$ ($\Delta G_{298} = -14$ kJ·mol$^{-1}$) or form isopropanol in complex **15** (triplet counterpart of **6**) through a rebound step (TS **14/15**). The release of propene by dehydration of propanol requires reorganization of the electronic distribution in the vanadium oxide moiety that is achieved by

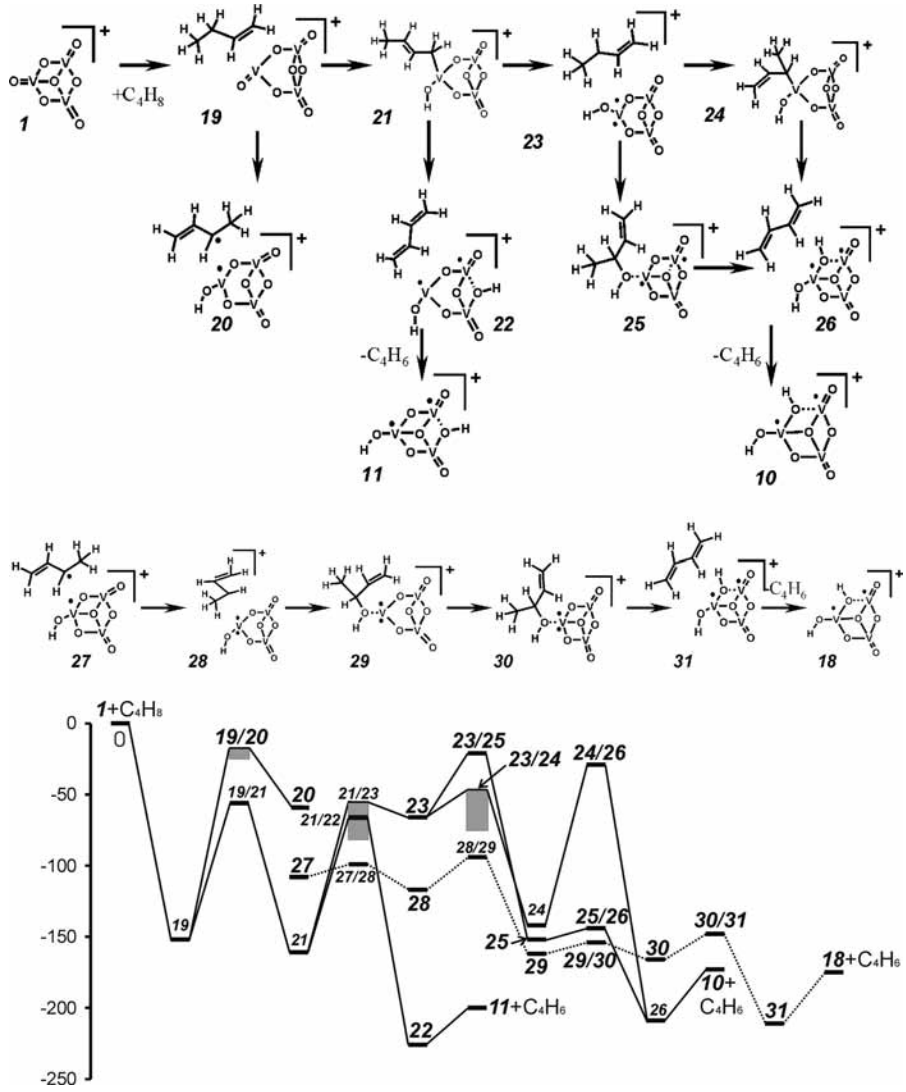


**Figure 5.** Reaction of but-1-ene with $V_3O_7^+$. Singlet (top) and triplet (middle) pathways and Gibbs free energy (298 K, kJ·mol$^{-1}$) reaction diagrams (bottom). The full and broken lines connect the singlet and triplet structures, respectively. The values (axis in kJ·mol$^{-1}$) are also reported in Table 2. The shaded areas indicate uncertainty intervals between broken-symmetry (bs) and spin-projected energies (s) when $\langle S^2\rangle_{bs}$ differs significantly from 1.

isomerization (TS **15/16**): ring-type $V_3O_6^+$ structure in **15**, cage-type $V_3O_6^+$ structure in **16**. Propene elimination (TS **16/17**) yields the complex **17** that is the triplet equivalent of the low-spin (singlet) structure **8**.

The main difference between the singlet and triplet reaction pathways is that in the former case formation of a C−V bond is observed (**4**) corresponding to C−H addition onto the V═O bond, whereas in the equivalent triplet structure the electron pair of the C−V bond is decoupled and forms a $C_3H_7^{\bullet}\cdot V_3O_7H^{\bullet+}$ diradical (**13**). Along **13/14**−**14/15**−**15/16** the triplet surface involves lower energies than the singlet one along **4/5**−**5/6**−**6/7**. At the end of the reaction (structures **16**−**17**−**18** compared to **7**−**8**−**10**) the differences become smaller and the two surfaces finally coincide.

**Reactions with But-1-ene.** Figure 5 shows the pathways for reactions of but-1-ene with $V_3O_7^+$ (top) together with the Gibbs free energy (298 K) profile (bottom). The energies and Gibbs free energies are reported in Table 2. The $V_3O_7^+$ ion binds but-1-ene much more strongly than propane ($\Delta G_{298} = -152$ vs $-63$ kJ·mol$^{-1}$) which is due to the specific interaction of the C═C bond with the coordinatively unsaturated O═V(O−)$_2^+$ site in the complex **19**. As with propane, hydrogen abstraction (TS **19/20**) is possible. The lower Gibbs free energy of **20**, −58 kJ·mol$^{-1}$ with respect to the reactants, compared to that of **3**, −22 kJ·mol$^{-1}$, reflects the lower C−H bond dissociation energy of but-1-ene compared to propane. Also the *apparent* free energy barriers of $-22 \pm 2$ kJ·mol$^{-1}$ (TS **19/20**) and $39 \pm 6$ kJ·mol-1 (TS **2/3**) suggest that H abstraction is "easier" from the allylic C−H bond in but-1-ene than from the C−H bond in propane. The *intrinsic* free energy barriers show the opposite relation, which is due to the much larger stability of **19** compared to **2**.

For both hydrocarbons, an alternative mechanism exists which corresponds to a formal [2 + 2] addition of a C−H bond onto the O═V bond of the O═V(O−)$_2^+$ site. For but-1-ene, the *intrinsic* Gibbs free energy barrier for the [2 + 2] addition (TS **19/21**) is 26 kJ·mol$^{-1}$ lower than that of propane (TS **2/4**). As result TS **19/21** is $32 \pm 2$ kJ·mol$^{-1}$ lower than TS **19/20**, and the [2 + 2] addition becomes the kinetically dominant reaction path with a $6 \times 10^5$ times larger rate constant. Intermediate **21** is an analogue of intermediate **4** for propane, but for propane the Gibbs free energy of the corresponding transition structure (TS **2/4**) is $20 \pm 6$ kJ·mol$^{-1}$ higher than that of the H abstraction (TS **2/3**), and hence kinetically not relevant. The O−H and C−V bonds in **4** will be formed either step-by-step in an asynchronous

**TABLE 2: Energies and Total Spin for the Reaction of But-1-ene with $V_3O_7^+$ [a]**

| label | $E_{el}$ | $E_0$ | $\Delta G_{298}$ | $\langle S^2 \rangle$ | $E_{spe}^{tr}$ |
|---|---|---|---|---|---|
| **1** + $C_4H_8$ | 0 | 0 | 0 | −/− | −/− |
| **19** | −203 | −199 | −152 | − | − |
| TS **19/20** | $-51^{bs}$, $-55^{s}$ | $-62^{bs}$, $-66^{s}$ | $-20^{bs}$, $-24^{s}$ | 0.87 | −47 |
| TS **19/21** | −95 | −108 | −56 | − | − |
| **20** | $-122^{bs}$, $-88^{s}$ | $-131^{bs}$, $-96^{s}$ | $-92^{bs}$, $-58^{s}$ | 1.01 | −156 |
| $V_3O_7H^{\bullet+}$ + $C_4H_7^{\bullet}$ | −16 | −28 | −29 | 0.76/0.78 | −/− |
| **21** | −208 | −210 | −161 | − | − |
| TS **21/22** | −110 | −125 | −66 | − | − |
| TS **21/23** | $-104^{bs}$, $-82^{s}$ | $-114^{bs}$, $-90^{s}$ | $-80^{bs}$, $-57^{s}$ | 0.97 | −128 |
| **22** | $-267^{bs}$, $-265^{s}$ | $-271^{bs}$, $-269^{s}$ | $-228^{bs}$, $-226^{s}$ | 1.02 | −269 |
| **11** + $C_4H_6$ | $-192^{bs}$, $-192^{s}$ | $-200^{bs}$, $-200^{s}$ | $-201^{bs}$, $-201^{s}$ | 1.03/− | −193/− |
| **23** | $-122^{bs}$, $-88^{s}$ | $-131^{bs}$, $-97^{s}$ | $-100^{bs}$, $-66^{s}$ | 1.01 | −156 |
| $V_3O_7H^{\bullet\bullet}$ + $C_4H_7^+$ | $-121^{bs}$, $-121^{s}$ | $-132^{bs}$, $-130^{s}$ | $-137^{bs}$, $-136^{s}$ | 1.02/− | −122 |
| TS **23/24** | $-101^{bs}$, $-76^{s}$ | $-110^{bs}$, $-85^{s}$ | $-74^{bs}$, $-48^{s}$ | 0.96 | −129 |
| TS **23/25** | $-105^{bs}$, $-60^{s}$ | $-111^{bs}$, $-66^{s}$ | $-67^{bs}$, $-21^{s}$ | 1.00 | −151 |
| **24** | −189 | −191 | −142 | − | − |
| TS **24/26** | −67 | −81 | −29 | − | − |
| **25** | $-206^{bs}$, $-205^{s}$ | $-199^{bs}$, $-198^{s}$ | $-153^{bs}$, $-152^{s}$ | 1.02 | −206 |
| TS **25/26** | $-170^{bs}$, $-168^{s}$ | $-185^{bs}$, $-183^{s}$ | $-145^{bs}$, $-144^{s}$ | 0.98 | −171 |
| **26** | $-254^{bs}$, $-253^{s}$ | $-257^{bs}$, $-256^{s}$ | $-210^{bs}$, $-209^{s}$ | 1.02 | −255 |
| **10** + $C_4H_6$ | $-166^{bs}$, $-165^{s}$ | $-174^{bs}$, $-173^{s}$ | $-174^{bs}$, $-173^{s}$ | 1.02/− | −167/− |
| $V_3O_7^{+\bullet\bullet}$ + $C_4H_8$ | 173 | 169 | 233 | 2.01/− | −/− |
| **27** | −146 | −153 | −108 | 2.03 | − |
| TS **27/28** | −143 | −149 | −99 | 2.03 | − |
| **28** | −157 | −162 | −117 | 2.03 | − |
| $V_3O_7H^{\bullet\bullet}$ + $C_4H_7^+$ | −130 | −138 | −140 | 2.01/− | −/− |
| TS **28/29** | −132 | −137 | −94 | 2.02 | − |
| **29** | −218 | −210 | −162 | 2.02 | − |
| TS **29/30** | −214 | −207 | −154 | 2.01 | − |
| **30** | −224 | −217 | −166 | 2.01 | − |
| TS **30/31** | −173 | −189 | −148 | 2.02 | − |
| **31** | −255 | −258 | −211 | 2.02 | − |
| **18** + $C_4H_6$ | −167 | −174 | −175 | 2.02/− | −/− |

[a] See Table 1.

mechanism via TS **2/3** and TS **3/4** if the biradical **3** is indeed an intermediate (as predicted by our B3LYP calculations), or in one step via TS **2/3**, should TS **3/4** disappear if more accurate methods are used.

From **21** but-1,3-diene is formed by a second H transfer. Because of the specific topologies of but-2-ene-yl and $[HOV_3O_6]^+$, the O atom that accepts the H atom from the $CH_3$ group in $C_4H_7$ (TS **21/22**) is one of the oxygen atoms in the V−O2−V four-membered ring (1−4 position with respect to the vanadium atom to which the butenyl group is bonded). Intermediate **22** is very stable with two electrons occupying d orbitals on different V sites that form an open-shell singlet state. Because of their weak interaction, the triplet state for the same geometric structure has almost the same energy (Table 2). After desorption of but-1,3-diene the same $V_3O_7H_2^{\bullet\bullet+}$ species **11** is obtained as after desorption of propene from **9**. The interaction energy between but-1,3-diene/propene and **11** is 69/59 kJ·mol$^{-1}$.

As with propane an alternative pathway from **21** exists that requires broken-symmetry calculations. It involves dissociation of the V−C bond (TS **21/23**) into the $C_4H_7^+ \cdot V_3O_7H^{\bullet\bullet}$ complex (**23**) between the neutral $V_3O_7H^{\bullet\bullet}$ species and the butenylium cation. As in the propane case this complex can dissociate into the hydride transfer products $V_3O_7H$ and $C_4H_7^+$ with a Gibbs free energy change of −70 kJ·mol$^{-1}$. From **23**, there are two additional pathways that ultimately lead to but-1,3-diene via intermediate **26**, but they involve transition structures, TS **23/25** (−21 kJ·mol$^{-1}$) and TS **24/26** (−29 kJ·mol$^{-1}$), with much higher Gibbs free energies than TS **21/22** (−66 kJ·mol$^{-1}$) and TS **19/21** (−56 kJ·mol$^{-1}$) on the closed shell pathway. The butenylium cation in **23** can rebind to the HO group of the $HO-V^{III}(O-)_2$ site (TS **23/25**) and form but-2-ol-3-ene as part of the $[C_4H_7OH \cdot V_3O_6^{\bullet\bullet}]^+$ complex (**25**). Crossing a small barrier (TS **25/26**) but-1,3-diene is formed in **26**.

The butenylium cation in **23** can also rebind to $V_3O_7H^{\bullet\bullet}$ via formation of a C−V bond (TS **23/24**) yielding intermediate **24,** an isomer of **21** that formally originates from a [2 + 2] addition of a different CH bond ($CH_2$ group instead of $CH_3$ group) to O═V. From this isomer but-1,3-diene can be formed by H transfer from the methyl group in a similar way as propene in step **4** to **8** (Figure 2). Dissociation of propene/but-1,3-diene leaves **10**. The isomerization through **23/24** is kinetically favored over but-2-ol-3-ene formation through **23/25**, but the *intrinsic* free energy barrier for the subsequent formation of but-1,3-diene from **24** is high, 113 kJ·mol$^{-1}$ (TS **24/26**).

Dissociation of complex **26** into but-1,3-diene and $V_3O_7H_2^{\bullet\bullet+}$ (**10**) requires 35 kJ·mol$^{-1}$. Species **10** is an isomer of **11** that has also two weakly interacting electrons in d-shells on two different vanadium atoms, but the two H atoms are at different oxygen positions (see Figure 1).

On the *triplet potential energy surface*, intermediate **27** is the counterpart of the singlet diradical **20**. The route through TS **27/28**, which corresponds to the transfer of an electron from $C_4H_7^{\bullet}$ to $HOV_3O_6^{\bullet+}$ yielding $C_4H_7^+$ and $HOV_3O_6^{\bullet\bullet}$, is the triplet analogue of that through TS **21/23**. Indeed, **23** and **28** differ only in their spin states. Both can dissociate into the butenylium cation (singlet) and $V_3O_7H$ (triplet). The Gibbs free energy of the separated products is −140 kJ·mol$^{-1}$.

Starting a triplet geometry optimization at the geometric structure of **21** leads to **27** in few cycles. The energy of **27** is higher than that of **21**, whereas the energy of the electron transfer

product **28** is lower than that of its singlet counterpart **23** (two electrons in d states on the same vanadium site prefer the triplet). Step **28/29**, rebinding of the butenylium cation onto O in the HO−V group, corresponds to step **23/25** on the singlet surface, and leads to but-2-ol-3-ene attached to $V_3O_6^+$ in **29**. A small barrier of only 8 kJ·mol$^{-1}$ separates **29**, which has a ring-type $V_3O_6^+$ part, from **30**, which has a cage-type $V_3O_6^+$ part with a 3-fold coordinated O. As found before with **25** and **7**, such isomer is required for the subsequent but-1,3-diene elimination in step **30/31**. The energies of TS **30/31** and **31** on the triplet surface are very close to those of TS **25/26** and **26**, respectively, on the (open shell) singlet surface (Figure 5 and Table 2). After desorption of but-1,3-diene, the same species **18** is obtained (triplet counterpart of **10**, Figure 1) as in the propane ODH. In summary, on the triplet reaction pathway, the energies of intermediates or TS from **27** to the products are lower than or similar to those on the singlet reaction pathway from **21**.

## Discussion

The mechanisms presented share crucial elementary steps with selective oxidation of C−H bonds by different transition metal oxide systems[27] ranging from gas phase species[28] to active sites of enzymes.[25] For example the oxidation of CH bonds to COH groups at the ferryl site in cytochrome P450 involves alcohol formation by rebinding the radical formed in the initial H abstraction to the HO−metal site,[25] similar to the formation of **6** and **15** for propane or **25** and **30** for but-1-ene. Below we discuss first the possible role of different spin states, and we then make comparison with mass spectrometric results for reactions of propane and but-1-ene with $V_3O_7^+$ and finally compare $V_nO_m^{+/0}$ gas phase species with O═V(O−)$_3$ surface sites in the ODH of propane.

**Role of Different Spin States.** $V_3O_7^+$ has a (closed shell) singlet ground state, and the $V_3O_7H_2^+$ product species have two electrons in d states of two different vanadium sites which form degenerate singlet and triplet states. Hence, the whole ODH reaction can occur on the singlet potential energy surface once the system has crossed the initial barrier for H abstraction (open shell singlet) in case of propane or for C−H addition (closed shell singlet) for but-1-ene. Hydride transfer can also be completed on the singlet potential energy surface. The $C_3H_7^+$/$C_4H_7^+$ cations are closed shell systems, and the (open-shell) singlet state of $V_3O_7H$ is (almost) degenerate with the triplet state although the two d electrons are on different vanadium sites in the singlet state, but on the same vanadium site in the triplet state.

The triplet potential energy surface could be entered from the singlet state of the reactants via the diradicaloid transition structures TS **2/3** (propane) or TS **19/20** (but-1-ene) around which the singlet and triplet potential energy surfaces are close to each other, leading to what has been called two-state reactivity.[25] For the propene and but-2,3-diene formation by a second hydrogen transfer, high energy transition structures (TS **4/8**, TS **4/9** and TS **21/22**, respectively) after intermediates **4** and **21**, respectively, could be avoided by crossing to the triplet potential energy surface. However, the qualitative reactivity pattern — no reaction with propane but ODH and hydride transfer with but-1-ene — will not change when considering crossings to the triplet potential energy surface. Predictions on which routes the systems would follow require localization of the minimum energy crossing points, see, e.g., ref 26, and calculating the transition probability between the singlet and triplet surfaces, but were beyond the scope of the present study.

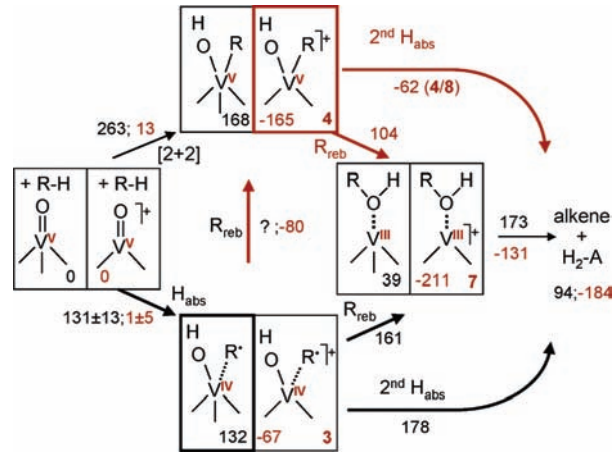


**Figure 6.** Comparison of O═V(O−)$_3$ surface sites (left boxes, black energy values) with $V_3O_7^+$ gas phase species (right boxes, red energy values, the bold numbers refer to the structures in Figure 2) in the ODH of propane. $H_2$-A is the reduced catalyst. Energies of intermediates (within the boxes) and of TS near the arrows are $E_0$ in kJ·mol$^{-1}$, black figures for O═V(O−)$_3$ surface sites, red figures for $V_3O_7^+$ gas phase ions.

**ODH of Propane and But-1-ene and Comparison with Experiment.** Two differences exist between the Gibbs free energy surfaces for the ODH of propane and but-1-ene. First, but-1-ene binds more strongly onto $V_3O_7^+$ than propane (−152 vs −63 kJ·mol$^{-1}$). The $\Delta G_{298}$ difference of 89 kJ·mol$^{-1}$ is almost completely due to the $\Delta E_0$ difference of 92 kJ·mol$^{-1}$. The *intrinsic* barriers for the first reactive steps are similar, 96 vs 102 ± 5 kJ·mol$^{-1}$ (91 vs 108 ± 5 kJ·mol$^{-1}$ for $\Delta E_0$). This brings the transition structure 56 kJ·mol$^{-1}$ below the reactants for but-1-ene, but creates an apparent barrier of 39 ± 5 kJ·mol$^{-1}$ for propane. This difference explains the mass spectrometric experiments in which ODH products are observed for but-1-ene only, but formation of the addition complex is observed for both but-1-ene and propane.[10] The apparent $E_0$ barrier for propane ODH is just 1 ± 5 kJ·mol$^{-1}$, and the apparent $G_{298}$ barrier of 39 ± 5 kJ·mol$^{-1}$ is largely due to the entropy gain connected with the dissociation of the addition complex in two species with rotational and translational degrees of freedom.

Second, the initial reactive steps are different. With but-1-ene the lowest barrier is obtained for a [2 + 2] addition of the C−H bond on the O═V bond, yielding an alkenyl group and an OH group attached to the same V site (**21**). With propane the same type of intermediate is reached (**4**), but in a two-step process. The first step is H abstraction from the C−H bond by the O═V group (homolytic C−H bond rupture) yielding a propyl radical, and in a second step the propyl radical rebinds to the V site (see also Figure 6). Apart from these differences, the following steps required to form but-1,3-diene and propene by a second hydrogen abstraction are rather similar.

For the reaction of $V_3O_7^+$ with but-1-ene formal hydride transfer has been observed in addition to ODH with a normalized product ratio of 14:54 = 0.26.[10b] For a reaction on the singlet potential energy surface the relevant barriers are connected with TS **21/23** and TS **21/22** (Figure 5) with $\Delta G_{298}$ values of −57 and −66 kJ·mol$^{-1}$, respectively, which implies a similar product ratio of 0.38.

**ODH of Propane by $V_nO_m^{+/0}$ Gas Phase Species and O═V(O−)$_3$ Surface Sites.** $V_3O_7^+$ is a closed-shell system with all vanadium atoms in the +V oxidation state. Comparison will be made with the smallest cation of this type, $VO_2^+$, whose reactions with propane have been studied both experimentally

**TABLE 3: B3LYP Barriers and Reaction Energies for the Reaction of Propane with Different Vanadium Oxide Species with Respect to Separated Reactants[a] and Energies for Model Reactions, $E_0$ in kJ·mol$^{-1}$**

| description | A = $VO_2^+$ | | A = $V_3O_7^+$ | A = $V_4O_{10}$ | A = O=V(O−)$_3$ |
|---|---|---|---|---|---|
| $C_3H_8$ + A | 0 | | 0 | 0 | 0 |
| RH···O=V($d^0$) | −168[b] | **2**[c] | −107 | 0[d] | 0[e] |
| TS H abstraction | − | **2/3**[c] | 1 ± 5 (108)[a] | 82[c] | 131 ± 13[e] |
| R•···HOV($d^1$) | − | **3**[c] | − 67 (40)[a] | 65[d] | 132[e] |
| TS CH addition | −59[b] (109) | **2/4**[c] | 13 (120)[a] | − | 263[e] |
| R(HO)V($d^0$) | −280[b] (−112) | **4**[c] | −165 (58)[a] | − | 168[e] |
| RO(H)•V($d^1$) | − | **7**[c] | −211 (−104)[a] | −76[d] | 39[e] |
| $C_3H_6$ + $H_2$-A | −167[b] | | −184 | −30[d] | 94[e] |
| model reactions | | | | | |
| 1/2 $H_2$ + O=V($d^0$)→ HOV($d^1$) | −196 | | −160 | −85 | −48 |
| $H_2$ + A→ $H_2$-A [g] | −317 | | −294 | −149 | −16 |
| A → $A_{O\text{-}def}$ + 1/2 $O_2$ | 114[f] | | 165[f] | 257[f] | 287[f] |

[a] In parentheses: intrinsic values with respect to the addition complex RH···O=V($d^0$). [b] Reference 12a. [c] See Figure 2 for numbering of intermediates and TS. [d] Reference 29. [e] Isolated vanadium oxide sites grafted on silica, ref 15a. [f] Reference 9a. [g] $H_2O$•V(O−)$_3$ species for the surface site, but dihydroxy species for all other.

and computationally by B3LYP.[12] Such calculations are also available for the ODH of propane by neutral $V_4O_{10}$ gas phase clusters[29] and by O=V(O−)$_3$ sites supported on silica.[15] The differences and similarities of these system may tell us what we can learn about surface reactions from gas phase experiments on clusters. Figure 6 compares the mechanisms for O=V(O−)$_3$ surface sites[15a] with that of $V_3O_7^+$ (this work), and Table 3 shows relevant energies at 0 K ($E_0$) for all systems.

The first difference is in *the binding of the substrate*, which is much stronger with cations, and particularly strong with the small $VO_2^+$ ion. Even for similar *intrinsic* barriers for $V_3O_7^+$ and O=V(OSi≡)$_3$ sites for the same initial H abstraction (108 ± 5 vs 132 ± 13 kJmol$^{-1}$) the *apparent* barriers become vastly different (1 ± 5 compared to 132 ± 13 kJ·mol$^{-1}$, Table 3). We should not forget, however, that gas phase reactions can *only* be observed if the (Gibbs free) energies of the transition structures are below the reactants (negative apparent barriers), whereas substantial barriers can be surmounted (depending on temperature) in condensed phase. The formation of the diradical intermediate R•···HOV($d^1$) from the addition complex RH···O=V($d^0$) requires more energy for O=V(OSi≡)$_3$ sites (132 kJ·mol$^{-1}$) than for $V_3O_7^+$ (40 kJ·mol$^{-1}$). The difference of 93 kJ·mol$^{-1}$ is largely due to the 112 kJ·mol$^{-1}$ difference between the hydrogenation energies,

$$\frac{1}{2}H_2 + O = V(d^0)HOV(d^1) \qquad (2)$$

The neutral gas phase cluster $V_4O_{10}$ is in between these two species, and for $VO_2^+$ the hydrogenation energy indicates an even higher reactivity.

After the initial H abstraction all subsequent TS have lower energies in the $V_3O_7^+$ case, contrary to what happens for the O=V(OSi≡)$_3$ surface site.[15a] There are electronic reasons for this, as indicated by the large difference in the reaction energies (−184 vs 94 kJ·mol$^{-1}$), but there are also steric reasons. A very stable *[2 + 2] CH addition complex*, R(HO)V, can be formed at the O=$V^+$(O−)$_2$ site of $V_3O_7^+$ (−165 kJ·mol$^{-1}$) extending the coordination on V from 3 to 4, whereas such an addition product on the O=V(OSi≡)$_3$ surface site (5-fold coordination on V including one isopropyl ligand) is unstable (168 kJ·mol$^{-1}$). This [2 + 2] CH addition complex is a central intermediate in the reactions with $V_3O_7^+$ from which the ODH products can be reached on different pathways. This intermediate is exceedingly stable for $VO_2^+$ (−280 kJ·mol$^{-1}$).

Table 3 shows also the energies of three model reactions that can be used to screen the activity of different vanadium oxide species A in ODH reactions.[9a,27] The hydrogenation energies,

$$H_2 + A \rightarrow H_2\text{-}A \qquad (3)$$

follow, of course, exactly the energies of the ODH reactions for a given hydrocarbon,

$$RCH_2CH_3 + A \rightarrow RCH = CH_2 + H_2\text{-}A \qquad (4)$$

as the data in Table 3 show. The O defect formation energies suggested previously as reactivity descriptor[9a] show the same trend.

The sequence of H attachment energies, eq 2, in Table 3 follows the energies of the transition structure for H abstraction $V_3O_7^+$ (1 ± 5) < $V_4O_{10}$ (82) < O=V(O−)$_3$ (131 ± 13 kJ·mol$^{-1}$). For $VO_2^+$ the H attachment energy is so low that a transition structure for H abstraction does not exist and C−H addition occurs with a very low barrier.

## Conclusions

The Gibbs free reaction energy profiles for the oxidative dehydrogenation of propane and but-1-ene by $V_3O_7^+$ show differences that are mainly due to the much more favorable interaction between the positively charged cluster and the double bond of the alkene. This results in apparent activation barriers that are negative for but-1-ene and positive for propane, which explains that ODH products are observed in experiments with the former, but not with the latter.[10] The central intermediate is a formal [2 + 2] adduct of the C−H bond onto the O=V bond of the O=$V^+$(O−)$_2$ site. Its stability with respect to the cation−hydrocarbon complex is due to the undercoordination of this site. With but-1-ene this adduct is formed in one synchronous step, while with propane the first step is hydrogen abstraction from the secondary C−H bond by the O=V group and subsequent rebinding of the propyl radical onto V. The calculations also explain the mass spectrometric observation[10b] of the butenylium cation as product of hydride transfer from but-1-ene to $V_3O_7^+$.

For reactions of propane with O=V(OSi≡)$_3$ sites on silica, similar steps are conceivable as for reactions with $V_3O_7^+$, but the reaction energy profile is different. The initial step is also hydrogen abstraction, but with a much higher barrier. Under

conditions of heterogeneous catalysis (fast reoxidation of vanadia sites), this step will be rate-determining,[15a] although — unlike the gas phase reactions considered here — barriers for subsequent steps are higher. Because of its high energy, the formal [2 + 2] adduct of the C−H bond onto the O═V bond does not play a role as intermediate on surfaces.

We find that energies of hydrogenation are a good descriptor of the energies of dehydrogenation reactions by oxide catalysts, and that H attachment energies can be used to predict within a set of related catalysts the sequence of energy barriers for the rate determining step.

**Acknowledgment.** This work was supported through an Alexander von Humboldt fellowship for X.R. and by the Deutsche Forschungsgemeinschaft (Collaborative Research Center 546 and Cluster of Excellence UNICAT).

**Supporting Information Available:** Cartesian coordinate files for structures presented in the manuscript. This material is available free of charge via the Internet at http://pubs.acs.org.

## References and Notes

(1) Böhme, D. K.; Schwarz, H. *Angew. Chem., Int. Ed.* **2005**, *44*, 2336–2354.

(2) (a) Marek, L. F. *Ind. Eng. Chem.* **1932**, *24*, 1103–1107. (b) Cullis, C. F. *Ind. Eng. Chem.* **1967**, *59*, 19–27.

(3) Limberg, C. *Angew. Chem., Int. Ed.* **2003**, *42*, 5932–5954.

(4) Wachs, I. E. *Catal. Today* **2005**, *100*, 79–94.

(5) (a) Wei, S.; Guo, B. C.; Purnell, J.; Buzza, S.; Castleman, A. W., Jr. *J. Phys. Chem.* **1992**, *96*, 4166–4168. (b) Bell, R. C.; Zemski, K. A.; Kerns, K. P.; Deng, H. T.; Castleman, A. W., Jr. *J. Phys. Chem. A* **1998**, *102*, 1733–1742.

(6) Asmis, K.; Brümmer, M.; Kaposta, C.; Santambrogio, G.; Von Helden, G.; Meijer, G.; Rademann, K.; Wöste, L. *Phys. Chem. Chem. Phys.* **2002**, *4*, 1101–1104.

(7) Asmis, K.; Meijer, G.; Brümmer, M.; Kaposta, C.; Santambrogio, G.; Wöste, L.; Sauer, J. *J. Chem. Phys.* **2004**, *120*, 6461–6470.

(8) Calatayud, M.; Andrés, J.; Beltrán, A. *J. Phys. Chem. A* **2001**, *105*, 9760–9775.

(9) (a) Sauer, J.; Döbler, J. *Dalton Trans.* **2004**, 3116–3121. (b) Asmis, K. R.; Sauer, J. *Mass Spectrom. Rev.* **2007**, *26*, 542–562.

(10) (a) Feyel, S.; Schröder, D.; Schwarz, H.; Rozanska, X.; Sauer, J. *Angew. Chem., Int. Ed.* **2006**, *45*, 4677–4681. (b) Feyel, S.; Schröder, D.; Schwarz, H. *J. Phys. Chem. A* **2006**, *110*, 2647–2654.

(11) Feyel, S.; Döbler, J.; Schröder, D.; Sauer, J.; Schwarz, H. *Angew. Chem., Int. Ed.* **2006**, *45*, 4681–4685.

(12) (a) Engeser, M.; Schlangen, M.; Schröder, D.; Schwarz, H.; Yumura, T.; Yoshizawa, K. *Organometallics* **2003**, *22*, 3933–3943. (b) Harvey, J. N.; Diefenbach, M.; Schröder, D.; Schwarz, H. *Int. J. Mass Spectrom.* **1999**, *182/183*, 85–97.

(13) (a) Gracia, L.; Andrés, J.; Safont, V. S.; Beltrán, A. *Organometallics* **2004**, *23*, 730–739. (b) Gracia, L.; Sambrano, J. R.; Safont, V. S.; Calatayud, M.; Beltrán, A.; Andrés, J. *J. Phys. Chem A* **2003**, *107*, 3107–3120.

(14) Bell, R. C.; Castleman, A. W. *J. Phys. Chem. A* **2002**, *106*, 9893–9899.

(15) (a) Rozanska, X.; Fortrie, R.; Sauer, J. *J. Phys. Chem. C.* **2007**, *111*, 6041–6050. (b) Rozanska, X.; Kondratenko, E. V.; Sauer, J. *J. Catal.* **2008**, *256*, 84–94. (c) Rozanska, X.; Sauer, J. *Int. J. Quantum Chem.* **2008**, *108*, 2223–2229.

(16) (a) Becke, A. D. *J. Chem. Phys.* **1993**, *98*, 5648–5652. (b) Lee, C.; Yang, W.; Parr, R. G. *Phys. Rev. B* **1988**, *37*, 785–789.

(17) Schäfer, A.; Huber, C.; Ahlrichs, R. *J. Chem. Phys.* **1994**, *100*, 5829–5835.

(18) (a) Ahlrichs, R.; Bär, M.; Häser, M.; Horn, H.; Kölmel, C. *Chem. Phys. Lett.* **1989**, *162*, 165–169. (b) Treutler, O.; Ahlrichs, R. *J. Chem. Phys.* **1995**, *102*, 346–354. (c) Eichkorn, K.; Weigend, F.; Treutler, O.; Ahlrichs, R. *Theor. Chem. Acc.* **1997**, *97*, 119–124. (d) Von Arnim, M.; Ahlrichs, R. *J. Chem. Phys.* **1999**, *111*, 9183–9190.

(19) Noodleman, L. *J. Chem. Phys.* **1981**, *74*, 5737–5743.

(20) Gräfenstein, J.; Hjerpe, A. M.; Kraka, E.; Cremer, D. *J. Phys. Chem. A* **2000**, *104*, 1748–1761.

(21) Wittbrodt, J. M.; Schlegel, H. B. *J. Chem. Phys.* **1996**, *105*, 6574–6577.

(22) (a) Pykavy, M.; van Wüllen, C.; Sauer, J. *J. Chem. Phys.* **2004**, *120*, 4207–4215. (b) Asmis, K. R.; Santambrogio, G.; Brümmer, M.; Sauer, J. *Angew. Chem., Int. Ed.* **2005**, *44*, 3122–3125.

(23) Pykavy, M.; van Wüllen, C. *J. Comput. Chem.* **2007**, *28*, 2252–2259.

(24) Bande, A.; Lüchow, A. *Phys. Chem. Chem. Phys.* **2008**, *10*, 3371–3376.

(25) Shaik, S.; De Visser, S. P.; Ogliaro, F.; Schwarz, H.; Schröder, D. *Curr. Opin. Chem. Biol.* **2002**, *6*, 556–567.

(26) Carreon-Macado, J.-L.; Harvey, J. N. *J. Am. Chem. Soc.* **2004**, *126*, 5789–5797.

(27) Sauer, J. In *Computational Modeling for Homogeneous and Enzymatic Catalysis*; Morokuma, K.; Musaev, D. G., Eds.; Wiley-VCH: Weinheim, 2008; pp 231−244.

(28) Fu, G.; Xu, X.; Lu, X.; Wan, H. *J. Phys. Chem. B* **2005**, *109*, 6416–6421.

(29) Cheng, M.-J.; Chenoweth, K.; Oxgaard, J.; Van Duin, A.; Goddard, W. A., III. *J. Phys. Chem. C* **2007**, *111*, 5115–5127.

JP9005235